Iranian Journal of Geophysics, Vol 18 No 3, 2024, Page 39 – 57 (Research Article)
DOI: 10.30499/IJG.2023.409210.1532

Formation evaluation of middle Miocene reservoirs via petrophysical analysis of well logging data; case study from Southern part of Gulf of Suez, Egypt

Mohammed Amer[1*], Walid M. Mabrouk [2], Khaled S. Soliman [2], Amr M. EID [1] and Ahmed Metwally [3]

[1] M.Sc.,Geophysics Department, Faculty of Science, Cairo University, Giza, Egypt
[2]Professor, Geophysics Department, Faculty of Science, Cairo University, Giza, Egypt
[3]Assistant Professor, Geophysics Department, Faculty of Science, Cairo University, Giza, Egypt

(Received: 13 September 2022, Accepted: 28 January 2023)

Abstract

The Amal oil field is located in the southern part of the Gulf of Suez and produces hydrocarbons mainly from middle Miocene reservoirs. It is marked by uncertainties in the southern part of the Gulf of Suez province because of the structural complexity, lateral facies change, different lithologies, and diverse reservoir quality. Therefore, in this approach, different reservoir properties of the Hammam Faraun Member of the Belayim Formation, the Markha Member of the Kareem Formation, and the Upper Rudies Member are obtained and evaluated. The main reservoirs are composed of sand and shale intercalations. The wireline logging data (gamma ray, density, neutron, sonic, and resistivity logs) of four wells were used mainly for the petrophysical analyses of hydrocarbon reservoirs. The three most important parameters in petrophysical evaluation: shale content, porosity, and fluid saturation are calculated for the main reservoirs to construct the litho-saturation model for each well. Each of these parameters is mapped to study their areal variation across the study area and estimate the appropriate locations for the new development wells. Fluid saturations are estimated based on the Indonesian formula due to shale presence. The study exhibited that Hammam Faraun, Markha, and Upper Rudies Formations have porosity of 0.15-0.17, 0.15-0.23, 0.12-0.27; shale volume of 0.3-0.36, 0.12-0.51, 0.19-0.37; and water saturation of 0.34-0.6, 0.33-0.51, 0.48-0.6, respectively. The results show an increasing trend toward the central part in porosity, sandy facies, and oil saturation. Based on the petrophysical evaluation and the mapping, the central part of the field is very promising for development and production activities.

Keywords: Southern Gulf of Suez, Middle Miocene reservoirs, petrophysical analysis, matrix identification, hydrocarbon indicators

*Corresponding author: mohamedamer@cu.edu.eg

1 Introduction

The Gulf of Suez is one of the most prolific basins in Egypt. Geologists and geophysicists are attracted to the oil and gas exploration in this basin because of the large subsurface sedimentary sections, which include considerable pre-Miocene and syn-Miocene reservoirs with huge amounts of hydrocarbons in the southern part of the Gulf of Suez rift underneath the evaporites of the post-rift stratigraphy with various trapping mechanisms. The Gulf of Suez contains mainly structural hydrocarbon traps, but stratigraphic traps and combined traps are also present (Alsharhan and Salah, 1994). The sandstone of the syn-rift Miocene strata contains about 60% of the hydrocarbon resources in the basin (Roberts, 2012).

The middle Miocene sediments have excellent hydrocarbon potential as sources, reservoirs, and seal rocks (Attia et al., 2015; Radwan et al., 2019). The middle Miocene succession is composed of six formations, namely, from base to top: Nukhul, Rudeis, Kareem, Belayim, South Gharib, and Zeit Formations. The sandstone of these formations has a good quality and a good history of hydrocarbon accumulation.

The eventual goal of the present study is to construct a petrophysical analysis by integrating the wireline logging data of 4 wells located in the southern part of the Gulf of Suez Province, to detect zones that are capable of accumulating hydrocarbons, as well as their depth and thickness, and to locate the contacts between oil, gas, and water within the pores of the Middle Miocene reservoirs in the study area that is bounded by latitudes 28° 02` N and 28°05` N and longitudes 33° 33` E and 33° 36` E (Fig.1). This case study focuses on the analysis of Hammam Faraun, a member of the Belayim formation, Markha, a member of the Kareem formation, and Upper Rudies, a member of the Rudies formation. These zones represent the syn-rift Miocene reservoir in the southern Gulf of Suez.

The petrophysical analysis of logging data is one of the most useful and significant tools for characterizing rock properties and evaluating zones of interest. The reservoir petrophysical parameters, such as its porosity, lithology, fluid saturation, and permeability, were obtained from logging data of density, gamma ray, neutron, shallow, and deep resistivity tools to evaluate the subsurface formations characteristics and determine the production rate of wells. (Hassan et al., 2014; Lyaka and Mulibo, 2018; Metwally et al., 2022; Chikiban et al., 2022).

2 Geological Settings

The Gulf of Suez rift basin was formed in the late Oligocene–early Miocene (Hempton, 1987). It is composed of three major half-grabens that have from north to south reversed dip polarity (Kassem et al., 2020). The major faults of the half grabens that are in the north and south directions dip toward the northeast direction (Radwan et al., 2021) and the strata within the tilted fault block have a dip toward the southwest direction. The major faults of the central half graben have a dipping direction toward the southwest direction, which is the opposite direction relative to the other grabens and the layers dip toward the northeastern direction (Patton et al., 1994). Two zones of accommodation separate the three half-grabens (Moustafa, 1976). Figure 1 represents the structural setting of the Gulf of Suez.

Stratigraphically, the Gulf of Suez is composed of rocks ranging from Precambrian to Holocene. These rocks are classified based on tectonic rift into 3 stratigraphic phases (Moustafa, 1976): (a) the pre-rift stratigraphic phase (pre-Miocene units) rest non-conformably on the basement rocks with ages ranging from Paleozoic to Eocene (Alsharhan, 2003); (b) the syn-rift stratigraphic phase (Miocene units), which is composed of sedimentary clastic units at the base of the section and

evaporitic facies at the top; (c) The post-rift stratigraphic phase (post-Miocene units) includes clastic rock units (Afifi et al., 2016).

Figure 2 represents the lithostratigraphic column of the Gulf of Suez's southern region. This study focuses mainly on middle Miocene reservoirs, the Belayim Formation, with more focus on the Hammam Faraun zone; the Kareem Formation, with more focus on the Markha zone (Patton et al., 1994); and the Upper Rudies Formation. Hammam Faraun is composed mainly of sandstone, shale intercalations, carbonate, and thin beds of anhydrite. Markha is composed of shales and sandstone intercalations. Rudies are composed mainly of shales with sandstone units (Shehata et al., 2021; Alsharhan, 2003).

Middle Miocene reservoirs represent approximately 20% of the Gulf of Suez's production (Patton et al., 1994). The source rocks of the study area may be from the Lower Miocene Rudeis and Kareem Formations and pre-rift units such as the shale of the Thebes Formation, the Sudr Formation, which is brown limestone, and the shale of the Matulla Formation (Alsharhan, 2003). Rudeis Formation may be an oil-prone source rock or an oil and gas-prone source rock (Afifi et al., 2016). The cap rock of the study area is mudstone and evaporites, both vertically and laterally. The mode of migration in the study area is hydrocarbon migration along faults or vertical migration from shale or carbonate source rocks. The trapping mechanism of the study area is a fault-bounded horst and a 3-way dip-closed fault-bounded trap (Alsharhan, 2003).

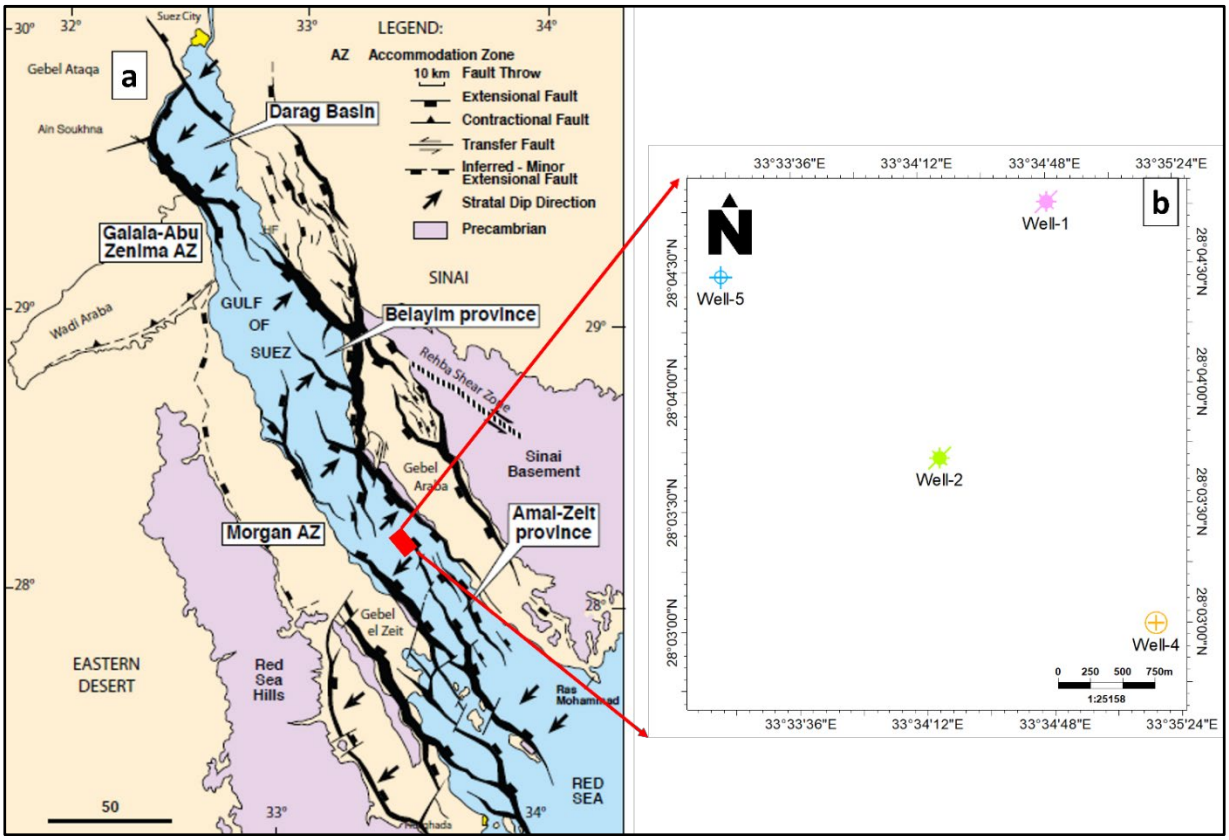

Figure 1. Location map of the study area (a) Gulf of Suez rift tectonic map (modified after Khalil, 1998). (b) A base map showing the available seismic lines and the four used well locations over the Amal field.

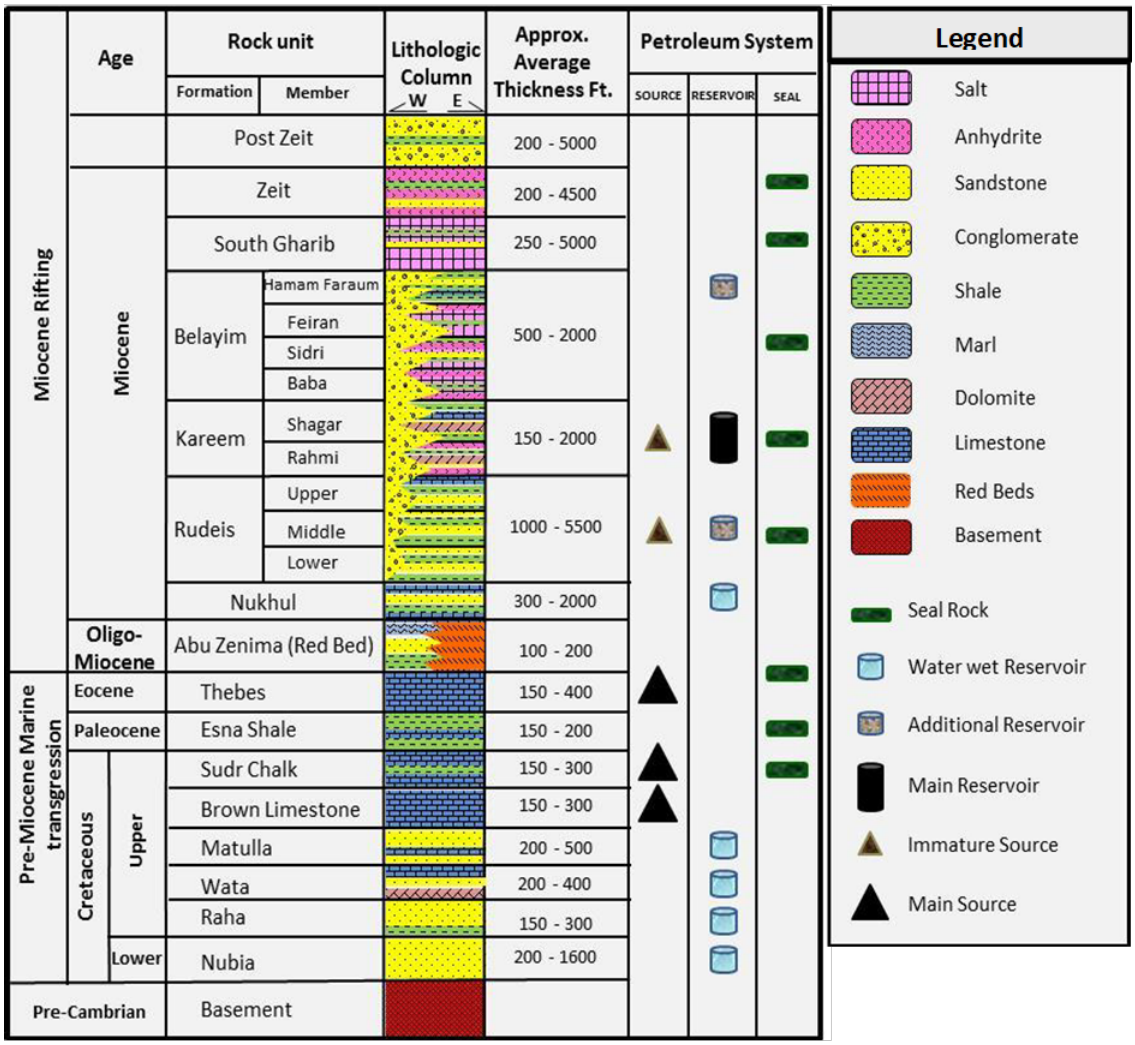

Figure 2. Stratigraphic column of the southern part of the Gulf of Suez (Mostafa et al., 2015).

3 Data and methodology

The available wireline logging data in this study is composed of logging data from four wells (Wells #1, #2, #3, and #4), including Gamma Ray logs, density logs, neutron logs, sonic logs, and resistivity logs, which were combined for the petrophysical analysis of Hammam Faraun Member/zone of Belayim Formation, Markha Member/zone of Kareem Formation, and Upper Rudies Formation. The petrophysical analysis starts with the detection of zones of interest based on defining the matrix type of each zone, determining which zones contain hydrocarbons based on the hydrocarbon indicators, calculating the resistivity of water (Rw) of selected zones based on the Pickett plot, and estimating the main petrophysical parameters (shale volume, total porosity, effective porosity, water saturation, bulk volume of water) to evaluate the reservoir quality (Faramani et al., 2019; Misaghi et al., 2021). Figure 3 represents the flow chart of the petrophysical analysis.

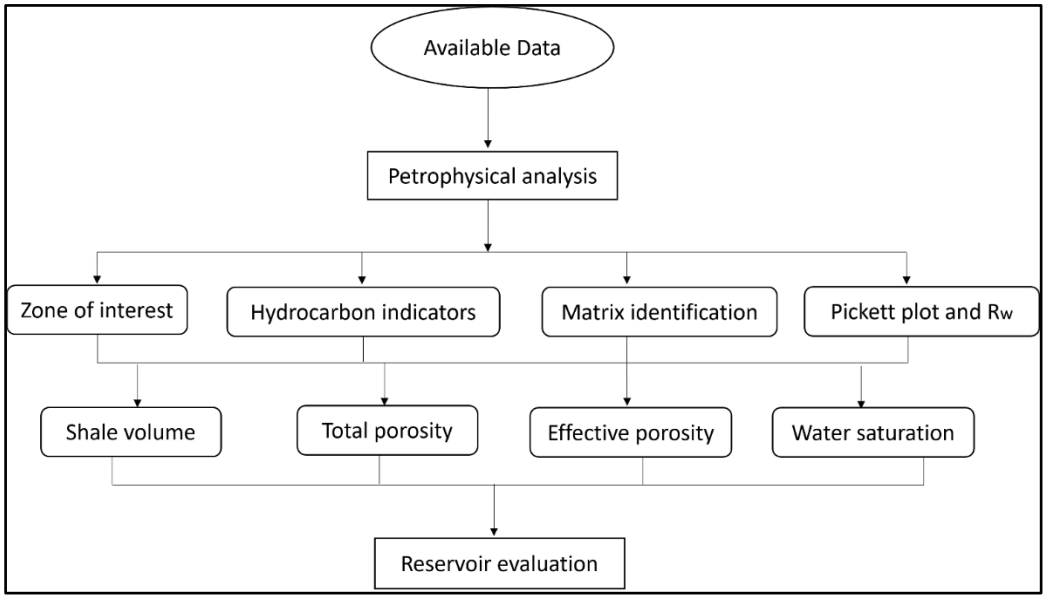

Figure 3. Flow chart of the petrophysical analysis.

3.1 Petrophysical analysis

The available well logs were analyzed to detect hydrocarbon bearing zones and to calculate the significant petrophysical parameters (shale content (V_{Shale}), total porosity (Φ_T), effective porosity (Φ_E), water saturation (S_w) and bulk volume of water (B_{VW})) within the zones of interest of Belayim Formation (Hammam Faraun Member/zone), Kareem Formation (Markha Member/zone), and Rudies Formation (Upper Rudies Member/zone) to perform the log-based petrophysical analysis.

3.1.1 Zone of interest

After the review of the logging data and the application of the log quality controls (L.Q.C.), the zones of interest were selected that have good petrophysical properties. The most significant parameter is the increase in the deep resistivity log, which is represented by the hydrocarbon presence. Also, the zone must reflect lower gamma-ray responses and the overlapping of density-neutron logs, which represent the permeable zone. Figure 4 shows an example of a zone of interest with low gamma rays, a curve separation between density and neutron logs, and an increase in the deep resistivity log.

3.1.2 Matrix identification

Two techniques were used to identify the matrix type of each zone, which are the M-N plot and the MID plot. The MID plot was used to identify matrix type according to the matrix density values (ρma) and the apparent value of matrix transit time (ΔTma). The matrix density and the matrix transit time were obtained based on the neutron, sonic, and density logs. By getting the intersection point of matrix density with matrix transit time on the MID chart, the matrix type can be identified.

The M-N plot was also used to identify the matrix based on calculating M and N values. M was calculated based on the sonic and density logs. N was calculated based on the neutron and density logs. M and N values were estimated based on the following equations (Hassan et al., 2014). By drawing the intersection point of M with N values, the matrix type can also be identified.

$$M = \frac{\Delta T_f - \Delta T_{log}}{\rho_b - \rho_f} * 0.01 \quad (1)$$

$$N = \frac{\emptyset_{Nf} - \emptyset_{N-log}}{\rho_b - \rho_f} \quad (2)$$

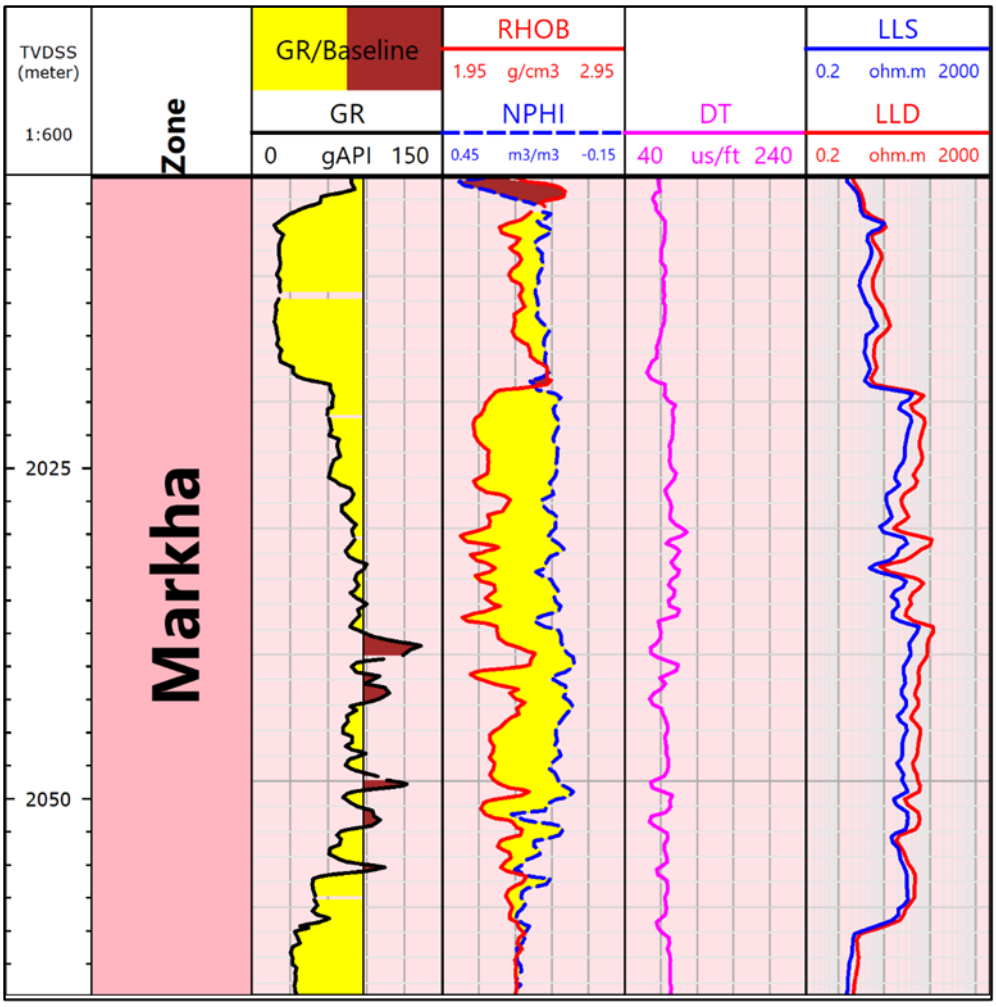

Figure 4. Full log display with an example of an interested zone.

Where ΔT_f is Transit time of fluid; ΔT_{log} Transit time of the formation; ρ_f Density of fluid; ρ_b Formation bulk density; $\emptyset_{Nf}$ Neutron porosity for fluid; $\emptyset_{N\text{-}log}$ Neutron porosity of the formation.

Matrix identification was constructed for three zones based on the two techniques (M-N plot, and MID plot). Hammam Faraun zone, Markha zone, and Upper Rudies zone are composed mainly of sand and shale intercalations, which is confirmed by the lithology interpretation of the logs. The M-N plot shows that the three zones are concentrated at the quartz region and approximate gas region, with many points toward the shale region, as shown in figure 5. Also, the MID plot shows that the three zones are concentrated in the quartz region with points in the shale region, as shown in figure 6. Both the M-N and MID plots show high consistency in their results.

3.1.3 Hydrocarbon indicators

Many techniques were developed to detect hydrocarbon-bearing zones, eliminate wet zones, and then make a detailed evaluation and examination of the hydrocarbon-bearing zones (Best et al., 1978; Fertl, 1978; Hassan et al., 2014). In this case study, we have used the (FR-Ro) formation resistivity factor (water resistivity) at water-bearing zone overlays (Mabrouk and Soliman, 2015), neutron-density overlays, and movable oil plots (MOP). In the case of the FR-Ro overlays, there will be a noticeable gap between Ro and FR in the hydrocarbon-bearing zone (Fig. 7c). Movable oil

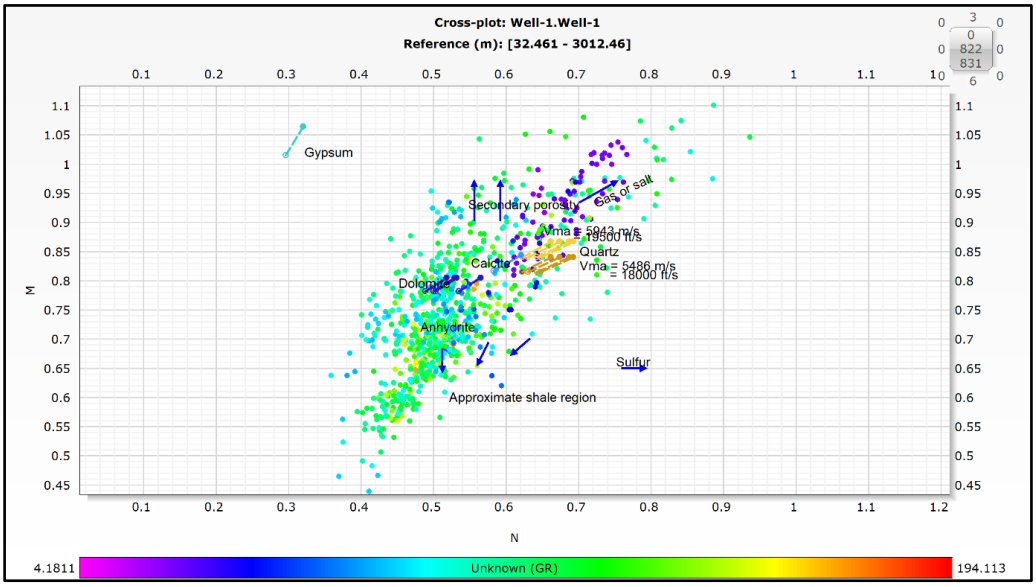

Figure 5. M-N cross plot for Hammam Faraun, Markha, and Upper Rudies.

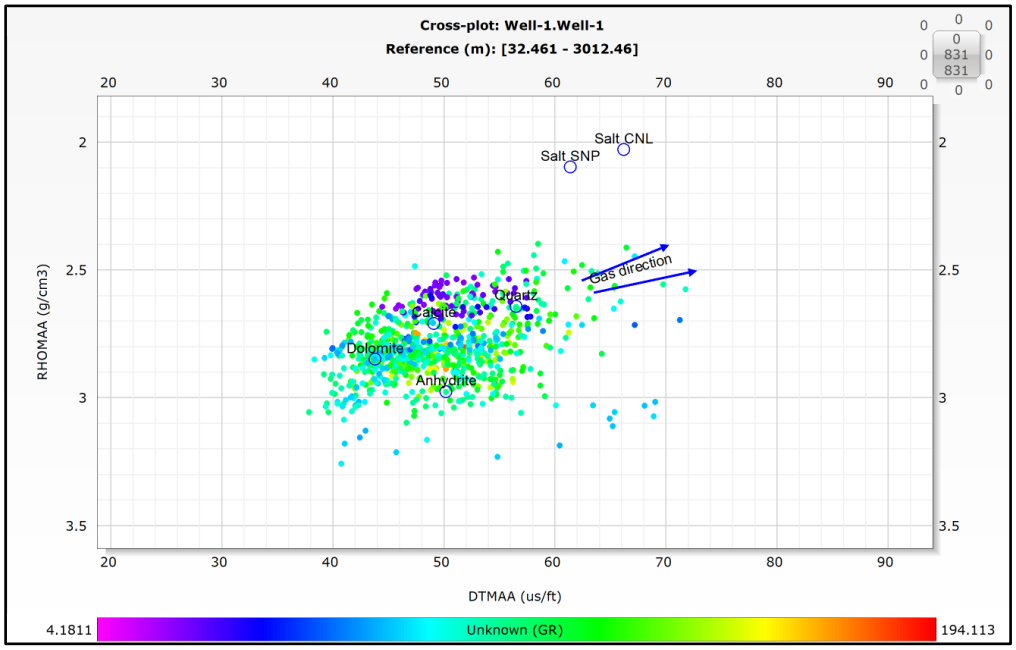

Figure 6. MID cross plot for Hammam Faraun, Markha, and Upper Rudies.

plots depend on plotting the invaded zone formation resistivity factor with the uninvaded zone formation resistivity factor. In the case of the movable hydrocarbon, we will have a noticeable curve separation between the two curves (Fig. 7b). Also, hydrocarbons can be detected from the separation between density and neutron logs (Fig. 7a). These three methods were used in the case study to detect the hydrocarbon in the Hammam Faraun, Markha, and Upper Rudies zones. Figure 7. Represent an example of three hydrocarbon indicators at the Markha zone. very good separation between the density and neutron log representing hydrocarbon presence, a noticeable gap between FR and Ro representing hydrocarbon presence, and a very good curve separation between the formation resistivity factor of invaded and uninvaded zones representing the movable hydrocarbon.

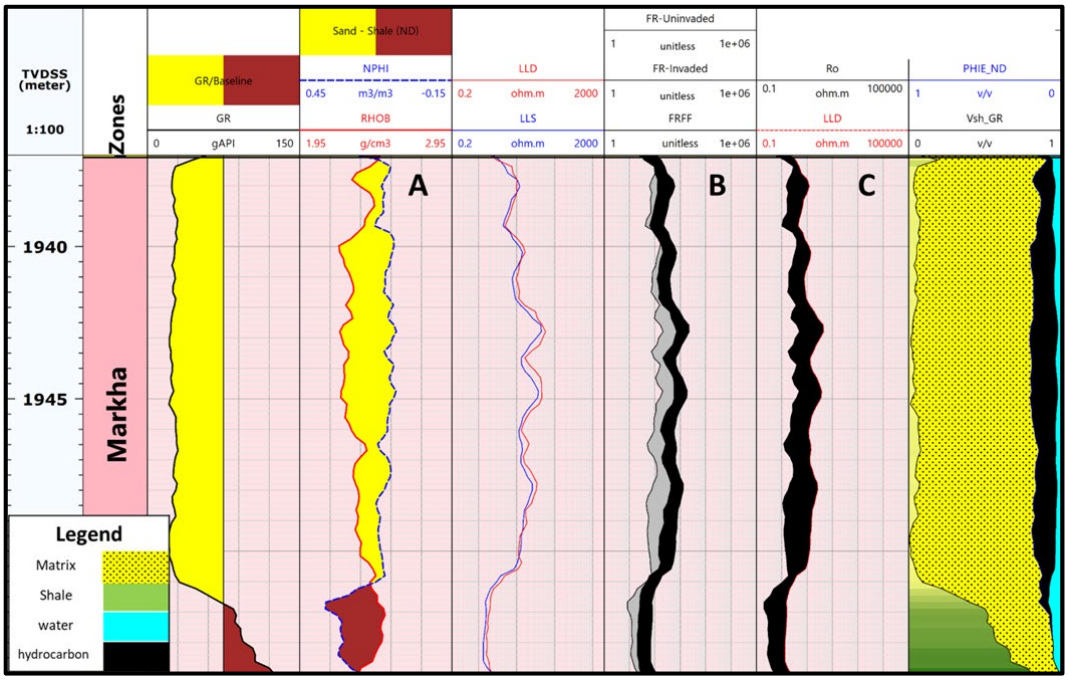

Figure 7. Hydrocarbon indicator techniques (a) Neutron-Density separation (b) movable oil plot (C) FR-Ro overlay.

3.1.4 Pickett plot and R_w calculations

The main purpose of the Pickett plot is to solve the Archie equation (Archie and others, 1942) without using any constants (Pickett, 1972). Based on the Pickett plot, which is a cross plot between resistivity and porosity, the water resistivity can be determined.

The Archie equation for formation resistivity factor (F), porosity ($\emptyset_N$), saturation of water (S_w), and water resistivity (R_w) in a rock is the following:

$$F = \frac{R_o}{R_w} = \frac{a}{\emptyset^m} \quad (3)$$

where: a is the proportionality constant; m is the cementation component; n is the saturation coefficient; R_o is the formation's resistivity at 100 percent water saturation; R_w is the water resistivity in the formation; and R_t is the accurate true formation resistivity.

Figure 7 shows the Pickett plot for Well #1, R_w was estimated from the plot at 100% porosity. In this case, the cut-off of the water saturation is 50%, so any zone over this value is considered to be a hydrocarbon-bearing zone, as shown in Figure 8. The R_w value of the main zones was 0.011ohm.m with a cementation exponent of two.

3.1.5 Shale volume (V_{sh})

Vsh is the most essential petrophysical parameter as it has a critical role in the calculation of the other petrophysical parameters like the effective porosity, fluid saturations, permeability, and net ratio, all of which are crucial for figuring out the reservoir quality, hydrocarbon potential, and realistic estimation of petroleum reserves. The shale volume in the three zones of interest was calculated according to the gamma-ray values as a linear response using the Asquith and Gibson equation (Asquith and Gibson, 1982):

$$Vsh = \frac{GR_{log} - GR_{min}}{GR_{max} - GR_{min}} \quad (4)$$

where V_{sh} is the shale volume; GR_{log} is the gamma-ray reading; GR_{max} is the maximum reading of gamma-ray; and GR_{min} is the minimum reading of gamma-ray.

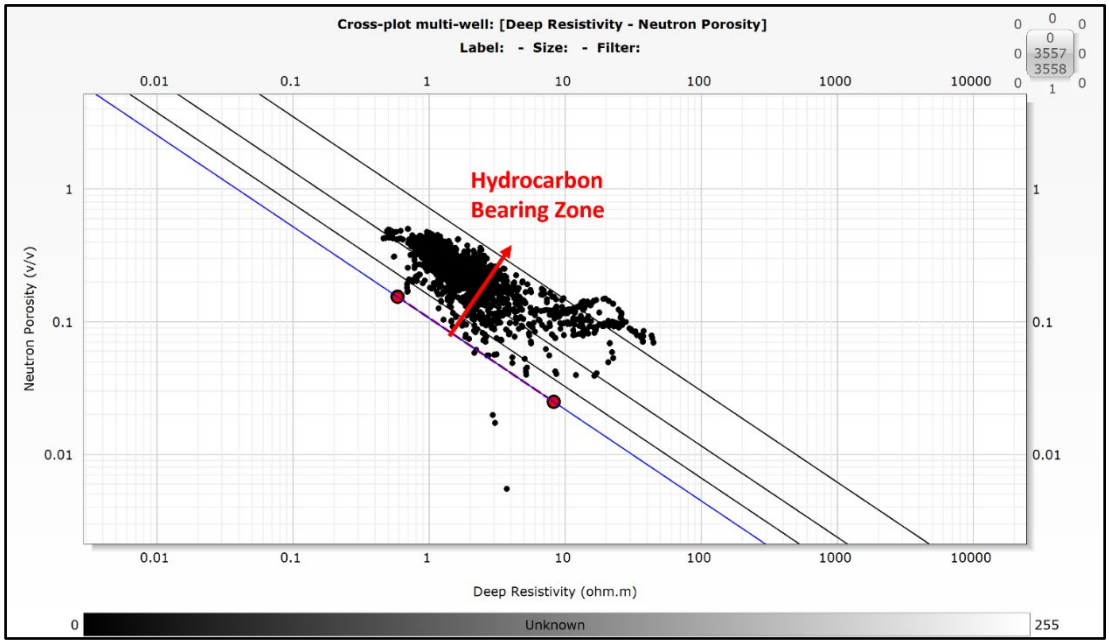

Figure 8. Pickett plot of Well #1.

3.1.6 Total porosity (ϕ_T)

Total porosity is the total amount of primary and/or secondary voids in the rocks. ϕ_T was estimated from the density-neutron logs based on the following equation after Asquith and Gibson (1982):

$$\emptyset_T = \frac{\emptyset_N + \emptyset_D}{2} \quad (5)$$

where Φ_T is the total porosity; Φ_N is the porosity from the neutron log; and Φ_D is the porosity from the density log.

The neutron porosity (Φ_N) is the amount of hydrogen inside the reservoir which is the value of the neutron log. In a clean reservoir (without shale) where the pores are filled by hydrocarbon or water, the neutron tool measures fluid-filled porosity (Φ_N). but the density porosity (Φ_D) can be estimated based on the following equation:

$$\emptyset_D = \frac{\rho_m - \rho_b}{\rho_m - \rho_{fl}} \quad (6)$$

where Φ_D is the porosity obtained from the density log; ρ_m is the density of matrix; ρ_b is the bulk density of rock; and ρ_{fl} is the density of fluids inside pores (mud fresh or salt, and hydrocarbons).

3.1.6 Effective porosity (ϕ_{eff})

The effective porosity is the volume of only interconnected pore spaces in rock through which fluids can flow (Stephens et al., 1998; Asquith and Gibosn, 1982). It was estimated based on the following formula:

$$\emptyset_{eff} = \emptyset_T - (V_{sh} * \emptyset_{sh}) \quad (7)$$

where Φ_{eff} is the effective porosity; Φ_T is the total porosity; V_{sh} is the shale volume; and Φ_{sh} is the shale porosity.

3.1.6 Water saturation (S_w)

The Indonesian formula (Poupon and Leveaux, 1971) was used to calculate water saturation for the important zones (Hammam Faraun, Markha, and Upper Rudies zones). The Indonesian model was used in this case because of the shale presence in the reservoirs. The water saturation can be estimated based on the following formula:

$$\frac{1}{\sqrt{R_t}} = \left[\sqrt{\frac{\varphi^m}{aR_w}} + \frac{V_{cl}^{\left(\frac{1-V_{cl}}{2}\right)}}{\sqrt{R_{cl}}}\right] {S_w}^n \quad (8)$$

Where S_w = water saturation, R_t = true resistivity, V_{cl} = clay or shale volume, $\emptyset_T$ = total porosity, $\emptyset_{sh}$ = shale porosity, a = tortuosity factor, R_w = formation water resistivity, and R_{cl} = resistivity of shale.

3.1.7 Bulk volume of Water saturation (BVW)

The bulk volume of water is one of the critical factors in evaluating the reservoir's quality. BVW can be calculated by using the product of porosity and water saturation. A certain zone can produce water-free hydrocarbons if its BVW is low and constant. It can be estimated based on the following equation (after Buckles, 1965):

$$BVW = SW * \emptyset_{eff} \quad (9)$$

Where BVW = bulk volume of water, S_w = water saturation, and $\emptyset_{eff}$ = effective porosity.

4 Results and discussion

4.1 Well correlation

The correlation was conducted for all the wells on the basis of the wireline logs. The correlation chart exhibits three major reservoir intervals with variable thickness throughout the formations of Belayim, Kareem, and Rudies, as shown in Figure 9. The three mentioned formations were recorded in all the drilled wells.

The Belayim Formation is subdivided into four zones: Hammam Faraun, Feiran, Sidri, and Baba members. Baba is composed of anhydrite and shale. Sidri is composed of salt, anhydrite, and shale. Feiran is composed of anhydrite and shale. Hammam Faraun is composed mainly of sandstone with shale intercalations.

Variable thicknesses of the Kareem Formation were recorded over the study area, which is composed of two members, the Markha and Shagar members. Shagar is composed mainly of shales with minor sand strikes. Markha is composed of sandstone with shale and streaks of anhydrite. Upper Rudies is composed mainly of shale and sandstone. Sandstones and shales of the Upper Rudeis Member extended over the entire area laterally with thickness variations with 70 m average thickness, ranging from 30 to 120 m thick due to structuration during the deposition that is related to Kareem-Rudeis unconformity (Okeil et al., 2019). The correlation results are in agreement with (Amer et al., 2023).

4.2 Petrophysical analysis

The logging data were analyzed using the Techlog geoscience platform to estimate the petrophysical parameters of the interested zones (Hammam Faraun, Markha, and Upper Rudies). Wireline logging data of neutron, density, resistivity, sonic, and gamma rays is used to estimate the total porosity, effective porosity, shale content, water saturation, hydrocarbon saturation, gross thickness, and net thickness of the target zone.

Vsh was calculated based on Eq. (4), with values that exhibit several variations. After the calculation, Vsh maps were constructed for the three zones. Hammam Faraun zone ranges from 0.3 to 0.36, which decreases toward the center of the area (Fig. 10a). Markha ranges from 0.12 to 0.28, with very low shale volume toward the northern part of the area (Fig. 10b). Upper Rudies range from 0.19 to 0.37, with low shale volume at the central part of the area (Fig. 10c). This variation may be due to the heterogeneity of the study area.

Effective porosity was calculated based on Eq. (7), with values exhibiting several varieties of increasing and decreasing. Three maps were constructed to track lateral variations of porosity. Hammam Faraun zone, ranging from 0.12 to 0.17, with very good porosity values toward the central part of the area (Fig. 10d). Markha ranging from 0.14 to 0.23, with maximum values at the central part of the area (Fig. 10e). Upper Rudies range from 0.1 to 0.27, with maximum values toward the northwestern part of the area (Fig. 10f). Very high variations in the values may be due to the heterogeneity of the facies in the study area. Effective porosity was calculated based on Eq. (7), with

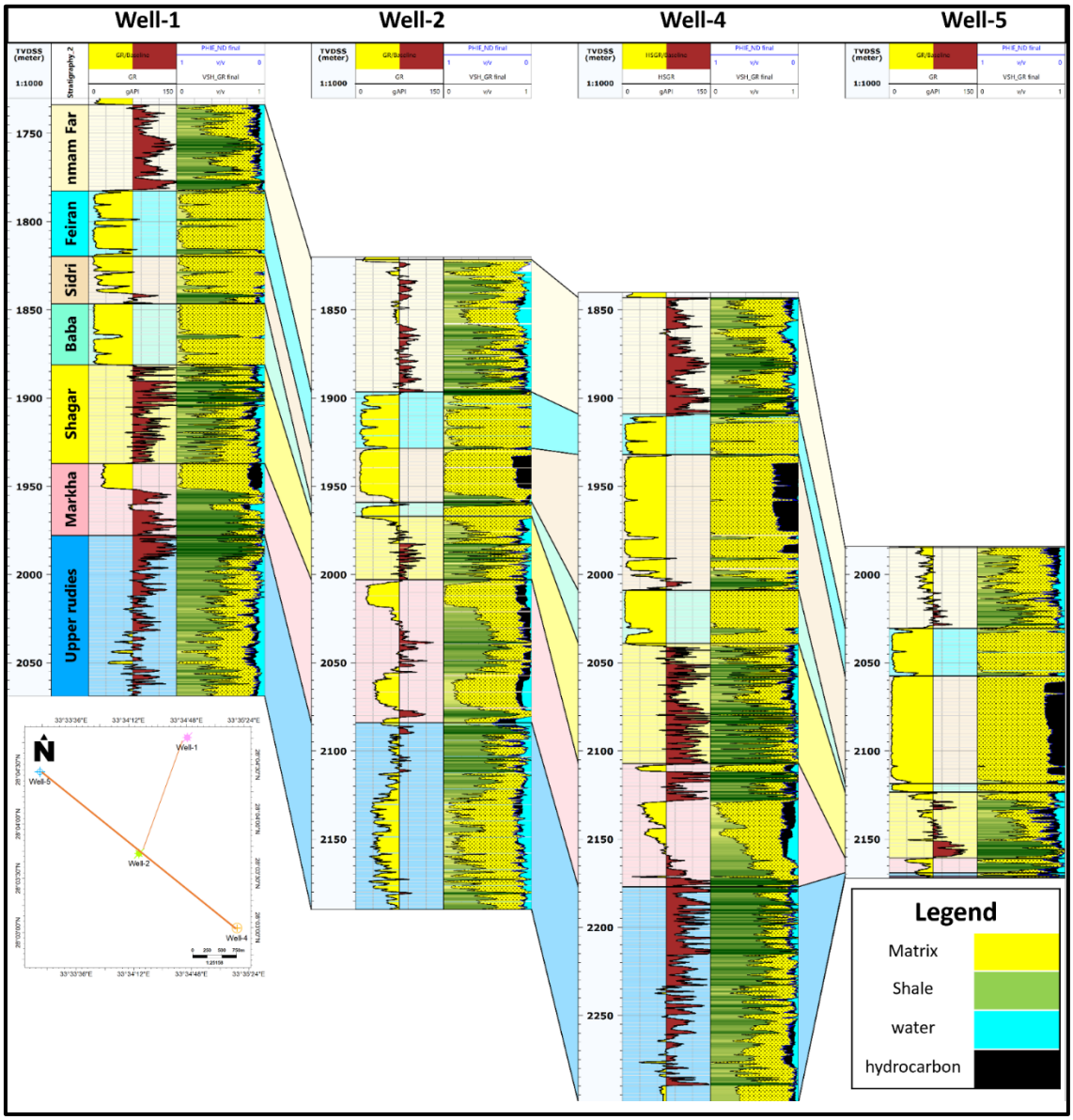

Figure 9. Well correlation showing log response The upper zone of Belayim is sand with shale intercalations; the lower zones are anhydrite with salt and shale; Kareem's upper zone is mainly shale, while the lower zone is sand with shale intercalations. The upper zone of Upper Rudies is composed of sandstone with shale intercalations.

Values exhibiting several varieties of increasing and decreasing. Three maps were constructed to track lateral variations of porosity. Hammam Faraun zone, ranging from 0.12 to 0.17, with very good porosity values toward the central part of the area (Fig. 10d). Markha ranging from 0.14 to 0.23, with maximum values at the central part of the area (Fig. 10e). Upper Rudies range from 0.1 to 0.27, with maximum values toward the northwestern part of the area (Fig. 10f). Very high variations in the values may be due to the heterogeneity of the facies in the study area.

Water saturation was calculated based on the Indonesian model Eq. (8) because of the shale presence in the three zones. Three water saturation maps were constructed to track lateral variations in the area, which may be because of the facies heterogeneity of the area. The value distribution exhibits several varieties of increasing and decreasing. Water saturation in the Hammam Faraun zone ranges from 0.34 to 0.6, with low saturation toward the northwestern part of the area (Fig. 11a).

Markha ranges from 0.33 to 0.51 with good water saturation values toward the northwestern part of the area (Fig. 11b). Upper Rudies range from 0.48 to 0.60, with low values at the southeastern and northwestern parts of the area (Fig. 11c).
The net pay of the three main zones was calculated based on the standard cut-off. Hammam Faraun zone, ranging from 23 to 28, with large sand thickness in the central part of the area (Fig. 11d). Markha ranging from 3 to 52, with a very large pay thickness at the central part of the area (Fig. 11e). Upper Rudies range from 2 to 47, with maximum pay thickness at the central part of the area (Fig. 11f). Table 1 represents the petrophysical analysis of the Hammam Faraun, Markha, and Upper Rudies reservoirs in the four studied wells. All the obtained petrophysical parameters show good agreement with (Abuel Ata et al., 2012; Ramadan et al., 2019; Farouk et al., 2022; Amer et al., 2023).

4.3 Litho-saturation model

It is the model that describes the composition of bulk rock volume, which is composed of three main petrophysical parameters (volume of shale, effective porosity, and bulk volume of water). From this model, the matrix percentage, shale volume, and percentage of hydrocarbon saturation can be estimated. The rock model is considered to be the end product of the petrophysical analysis used for the interpretation.

The rock model was constructed for the three formations (Belyaim, Kareem, and Upper Rudies); the case study focused only on the three main zones (Hammam Faraun Member of Belayim, Markha Member of Kareem, and Upper Rudies Formation) with good petrophysical parameters and considered to be hydrocarbon-bearing zones according to the litho-saturation model (Fig. 9). This rock model is in agreement with (Amer et al., 2023).

Table 1. Petrophysical analysis of the study area.

Parameters	Wells	Well #1	Well #2	Well #3	Well #4	Well #5
	Zone					
Volume of shale (Vsh) %	Hammam Faraun	0.34	0.36	0.29	0.33	0.29
	Markha	0.13	0.32	0.28	0.26	0.21
	Upper Rudies	0.36	0.27	0.21	0.37	0.14
Total porosity (phit) %	Hammam Faraun	0.24	0.24	0.26	0.23	0.20
	Markha	0.24	0.18	0.22	0.20	0.24
	Upper Rudies	0.26	0.25	0.26	0.22	0.20
Effective porosity (phie) %	Hammam Faraun	0.14	0.16	0.185	0.12	0.16
	Markha	0.18	0.15	0.23	0.16	0.19
	Upper Rudies	0.14	0.16	0.19	0.09	0.27
Water saturation (Sw) %	Hammam Faraun	0.45	0.49	0.367	0.62	0.46
	Markha	0.33	0.42	0.51	0.42	0.42
	Upper Rudies	0.58	0.62	0.57	0.48	0.51

Hydrocarbon saturation (Sh) %	Hammam Faraun	0.55	0.51	0.64	0.38	0.54
	Markha	0.67	0.58	0.49	0.58	0.58
	Upper Rudies	0.42	0.38	0.43	0.52	0.49
Gross thickness	Hammam Faraun	48	75	68.5	66	46
	Markha	45	81	88	75	10
	Upper Rudies	95	100	15	122	2

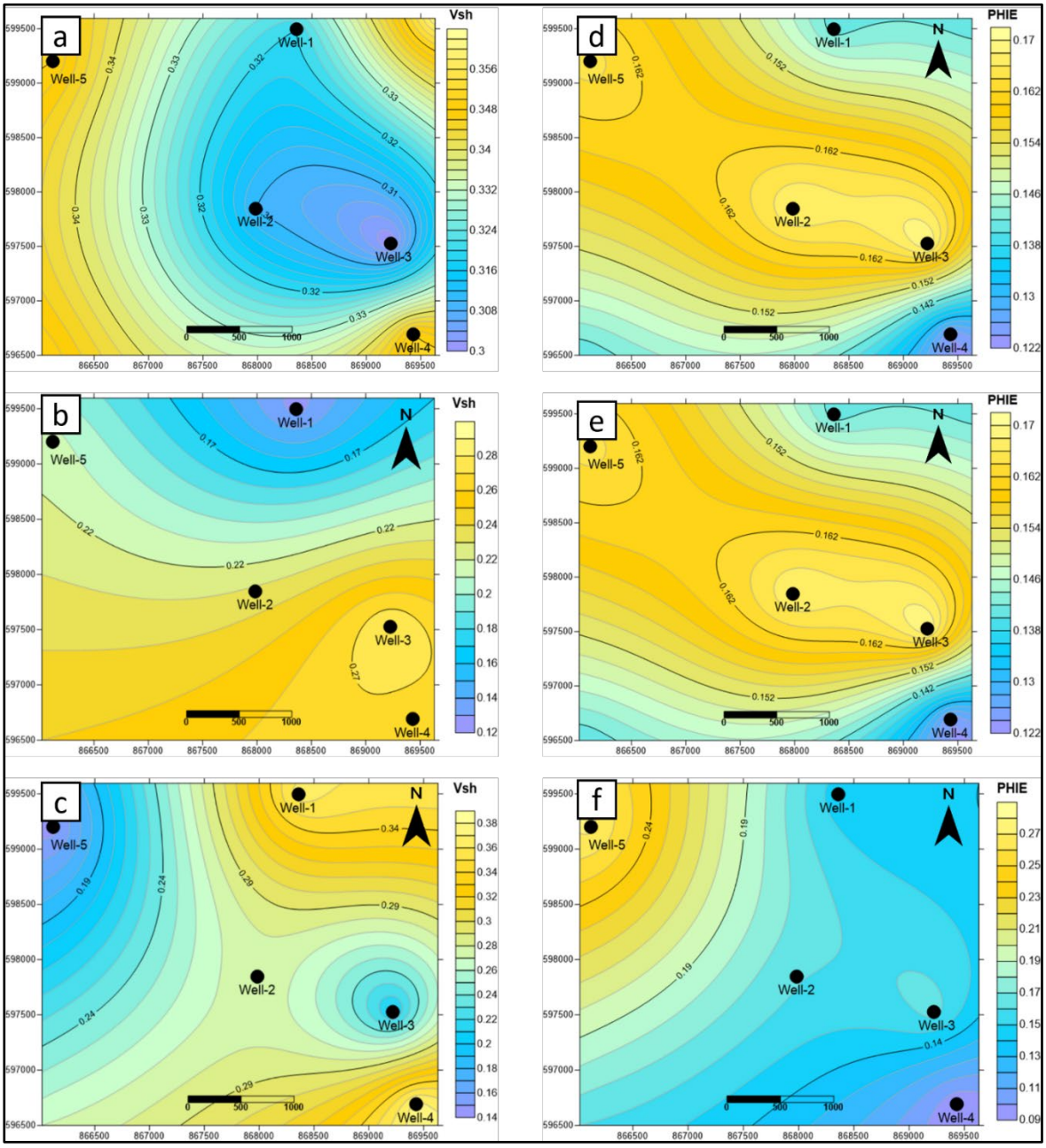

Figure 10. Vsh map of (a) the Hammam Faraun zone, (b) the Markha zone, and (c) the upper rudies; effective porosity map of (d) the Hammam Faraun zone, (e) the Markha zone and (c) the upper rudies.

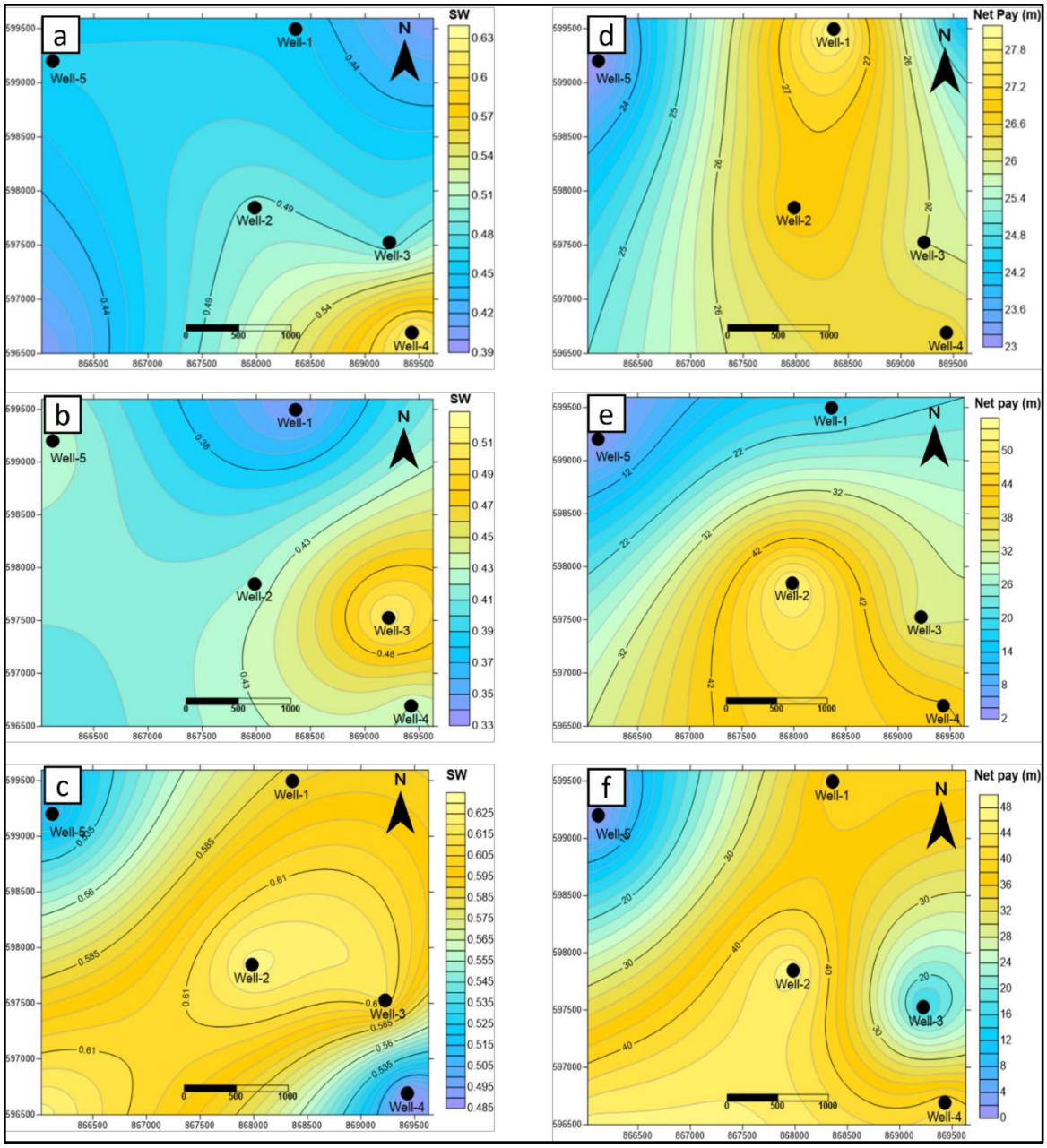

Figure 11. Water saturation map of (a) the Hammam Faraun zone, (b) the Markha zone, and (c) the upper rudies; net pay map of (d) the Hammam Faraun zone, (e) the Markha zone and (c) the upper rudies.

4.3 Seismic data interpretation

The seismic data analysis consists of four major steps: (1) formation tops detection and seismic to well tie; (2) delineating horizons laterally with fault detection; (3) closing loops and creating geo-cross sections; and (4) creating different sorts of geological maps to describe geological features. (Nanda and Nanda, 2016; Abuzaied et al., 2019; Noureldin et al., 2023). The main objective is to discover oil and gas accumulations, track their lateral extent, and estimate their amounts (Avseth et al., 2010). Three formation tops, the Belayim Formation, the Kareem Formation, and the Upper Rudies Formation, are picked out and tracked laterally in the seismic sections. Faults are interpreted and tracked in all the seismic sections. The interpreted seismic section exhibits a main horst structure bounded by two major faults extending along the area

trending northeast-southwest (clysmic trend), affected by minor faults (Fig. 12). All the major and minor faults affect the three reflectors: Belayim, Kareem, and Rudies Formations. two major faults. One of the major faults throws northeast with a large displacement and is branched into smaller faults in the northern part of the area, and the other throws southwest with a smaller displacement relative to the northeast fault. The obtained interpretation shows good agreement with (Okeil et al., 2019).

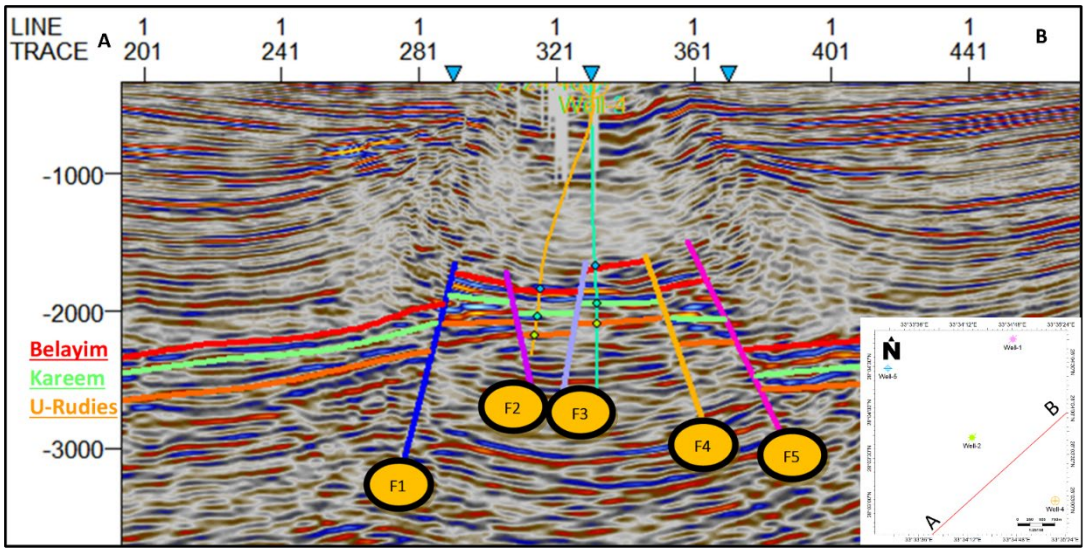

Figure 12. Interpreted seismic section from the southern part of the area.

4.4 Petroleum system

There are three major reservoirs in the study area: the Rudies Formation, the Kareem Formation, and the Belayim Formation. Rudies reservoirs represent approximately 20% of the Gulf of Suez's production potential, Kareem Formation sandstones are one of the best hydrocarbon reservoirs in the Gulf of Suez, producing and/or testing hydrocarbon from many different locations; and Belayim formations represent around 10.5% of the Gulf of Suez's oil production. The source of the study area may be from the lower Miocene Rudeis Formation and Kareem Formation or from pre-rift units such as the shale of the Thebes Formation, brown limestone of the Sudr Formation, and shale of the Matulla Formation. The Rudeis Formation may be an oil-prone source rock or an oil-and-gas-prone source rock. The cap rock of the study area is mudstone and evaporites, both vertically and laterally. The mode of migration in the study area is hydrocarbon migration along faults or vertical migration from shale or carbonate source rocks. The trapping mechanisms of the study area are fault-bounded horsts and 3-way dip closed fault-bounded traps (Alsharhan, 2003). The study area contains a promising petroleum system with good physical properties, so we highly recommend drilling more development wells. According to the study, two additional prospect areas can be identified that offer a good location for hydrocarbon accumulation (Figure 12).

5 Conclusion

The main goal of the current study was the interpretation of geological and geophysical data to assess the lithofacies and petrophysical characteristics of Middle Miocene reservoirs in the southern Gulf of Suez, as well as their distribution. In order to estimate the distribution and quality of the intricate Middle Miocene reservoirs and to lessen uncertainty during oilfield

development in the research area, we employed integrated datasets in this work. The primary results of this investigation were as follows:

Pay thickness maps were constructed for the Hammam Faraun, Markha, and Upper Rudies zones. The sand pay thickness of Hammam Faraun Member ranges from 23 m to 28 m, that of Markha Member ranges from 3 m to 52 m, and that of Upper Rudies Member ranges from 2 m to 47 m.

The petrophysical analysis shows that the central part of the area is a potential area with good reservoir properties. The analysis results of the area show that the Hammam Faraun zone is a good reservoir, with porosity values ranging from 0.15 to 0.23, Vsh ranging from 0.29 to 0.36, Sw ranging from 0.34 to 0.49, and net pay thickness ranging from 23 m to 28 m.

The Markha zone is also a good reservoir, with porosity values ranging from 0.14 to 0.23, Vsh ranging from 0.13 to 0.29, Sw ranging from 0.33 to 0.51, and net pay thickness ranging from 3 m to 52 m.

Upper Rudies exhibit good reservoir properties with porosity values ranging from 0.1 to 0.27, Vsh ranging from 0.19 to 0.37, Sw ranging from 0.48 to 0.60, and net pay thickness ranging from 3 m to 33 m.

After the petrophysical analysis and lateral distribution of petrophysical parameters according to the constructed maps, we highly recommend drilling more development wells in that area.

References

Abuel Ata, A. S. A., Azzam, S. S. S., and El-Sayed, N. A. A. (2012). The improvements of three-dimensional seismic interpretation in comparison with the two-dimensional seismic interpretation in Al-Amal oil field, Gulf of Suez, Egypt. Egyptian Journal of Petroleum, 21(1). https://doi.org/10.1016/j.ejpe.2012.02.004

Abuzaied, M., Metwally, A., Mabrouk, W., Khalil, M., and Bakr, A. (2019). Seismic interpretation for the Jurassic/Paleozoic reservoirs of QASR gas field, Shushan-Matrouh basin north Western Desert, Egypt. Egyptian Journal of Petroleum, 28(1). https://doi.org/10.1016/j.ejpe.2018.12.008

Afifi, A. S., Moustafa, A. R., and Helmy, H. M. (2016). Fault block rotation and footwall erosion in the southern Suez rift: Implications for hydrocarbon exploration. Marine and Petroleum Geology, 76, 377–396.

Alsharhan, A. S. (2003). Petroleum geology and potential hydrocarbon plays in the Gulf of Suez rift basin, Egypt. AAPG Bulletin, 87(1).

Alsharhan, A. S., and Salah, M. G. (1994). Geology and hydrocarbon habitat in a rift setting: southern Gulf of Suez, Egypt. Bulletin of Canadian Petroleum Geology, 42(3).

Amer, M., Mabrouk, W. M., Soliman, K. S., Noureldin, A. M., and Metwally, A. (2023). Three-Dimensional Integrated Geo-Static Modeling for Prospect Identification and Reserve Estimation in the Middle Miocene Multi-Reservoirs: A Case Study from Amal Field, Southern Gulf of Suez Province. Natural Resources Research. https://doi.org/10.1007/s11053-023-10253-w

Archie, G. E., and others. (1942). The electrical resistivity log as an aid in determining some reservoir characteristics. Transactions of the AIME, 146(01).

Asquith, G. B., and Gibosn, C. R. (1982). Basic well log analysis for geologists. American Association of Petroleum Geologists.

Attia, M. M., Abudeif, A. M., and Radwan, A. E. (2015). Petrophysical analysis and hydrocarbon potentialities of the untested Middle Miocene Sidri and

Baba sandstone of Belayim Formation, Badri field, Gulf of Suez, Egypt. Journal of African Earth Sciences, 109. https://doi.org/10.1016/j.jafrearsci.2015.05.020

Avseth, P., Mukerji, T., Mavko, G., and Dvorkin, J. (2010). Rock-physics diagnostics of depositional texture, diagenetic alterations, and reservoir heterogeneity in high-porosity siliciclastic sediments and rocks - A review of selected models and suggested work flows. Geophysics, 75(5). https://doi.org/10.1190/1.3483770

Best, D. L., Gardner, J. S., and Dumanoir, J. L. (1978). A computer-processed wellsite log computation. SPWLA Annual Logging Symposium, SPWLA–1978.

Buckles, R. S. (1965). Correlating and Averaging Connate Water Saturation Data. Journal of Canadian Petroleum Technology, 4(01). https://doi.org/10.2118/65-01-07

Chikiban, B., Kamel, M. H., Mabrouk, W. M., and Metwally, A. (2022). Petrophysical characterization and formation evaluation of sandstone reservoir: Case study from Shahd field, Western Desert, Egypt. Contributions to Geophysics and Geodesy, 52(3). https://doi.org/10.31577/congeo.2022.52.3.5

Faramani, E. R., Riahi, M. A., and Hashemi, H. (2019). Constrained seismic sequence stratigraphy of Asmari - Kajhdumi interval with well-log Data. Iranian Journal of Geophysics, 12(5).

Farouk, S., Sen, S., Pigott, J. D., and Sarhan, M. A. (2022). Reservoir characterization of the middle Miocene Kareem sandstones, Southern Gulf of Suez Basin, Egypt. Geomechanics and Geophysics for Geo-Energy and Geo-Resources, 8(5), 130.

Fertl, W. H. (1978). Practical log analysis. Part 8. R/sub wa/method: fast formation evaluation. Oil Gas J.;(United States), 76.

Hassan, A. M., Mabrouk, W. M., and Farhoud, K. M. (2014). Petrophysical analysis for Ammonite-1 well, Farafra Area, Western Desert, Egypt. Arabian Journal of Geosciences, 7(12). https://doi.org/10.1007/s12517-013-1123-y

Hempton, M. R. (1987). Constraints on Arabian Plate motion and extensional history of the Red Sea. Tectonics, 6(6). https://doi.org/10.1029/TC006i006p00687

Kassem, A. A., Sharaf, L. M., Baghdady, A. R., and El-Naby, A. A. (2020). Cenomanian/Turonian oceanic anoxic event 2 in October oil field, central Gulf of Suez, Egypt. Journal of African Earth Sciences, 165. https://doi.org/10.1016/j.jafrearsci.2020.103817

Khalil, S. M. (1998). Tectonic evolution of the eastern margin of the Gulf of Suez, Egypt. Royal Holloway, University of London.

Lyaka, A., and Mulibo, G. (2018). Petrophysical Analysis of the Mpapai well Logs in the East Pande Exploration Block, Southern Coast of Tanzania: Geological Implication on the Hydrocarbon Potential. Open Journal of Geology, 8, 781–802.

Mabrouk, W. M., and Soliman, K. S. (2015). A numerical technique for an accurate determination of formation resistivity factor using FR-RO overlays method. Arabian Journal of Geosciences, 8(3). https://doi.org/10.1007/s12517-014-1311-4

Metwally, A. M., Mabrouk, W. M., and Mahmoud, A. I. (2022). A numerical approach to accurately estimate water resistivity (Rw) and saturation (Sw) in shaly sand formations. Contributions to Geophysics and Geodesy, 52(3), 423–441. https://doi.org/10.31577/congeo.2022.52.3.4

Misaghi, A., Anvari, L., and Asef, M. R.

(2021). Porosity estimation of gas reservoir rocks using vertical seismic profiling data- a case study in the Persian Gulf. Iranian Journal of Geophysics, 15(2). https://doi.org/10.30499/ijg.2021.284833.1327

Mostafa, A., Sehim, A., and Yousef, M. (2015). Unlocking subtle hydrocarbon plays through 3D seismic and well control: A case study from west Gebel El Zeit district, southwest Gulf of Suez, Egypt. Offshore Mediterranean Conference and Exhibition, OMC 2015.

Moustafa, A. M. (1976). Block faulting in the Gulf of Suez. Proceedings of the 5th Egyptian General Petroleum Corporation Exploration Seminar, 35.

Nanda, N. C., and Nanda, N. C. (2016). Seismic Wave Propagation and Rock-Fluid Properties. Seismic Data Interpretation and Evaluation for Hydrocarbon Exploration and Production: A Practitioner's Guide, 3–17.

Noureldin, A. M., Mabrouk, W. M., Chikiban, B., and Metwally, A. (2023). Formation evaluation utilizing a new petrophysical automation tool and subsurface mapping of the Upper Cretaceous carbonate reservoirs, the southern periphery of the Abu-Gharadig basin, Western Desert, Egypt. Journal of African Earth Sciences, 205. https://doi.org/10.1016/j.jafrearsci.2023.104977

Okeil, M., Sakran, S., Refaat, A., El-Gamil, S., and Ramzy, M. (2019). INTEGRATED GEOLOGICAL INTERPRETATION FOR MODELING THE COMPLICATED RESERVOIRS; AN EXAMPLE FROM UPPER RUDEIS AND KAREEM RESERVOIRS, AMAL FIELD, SOUTHERN GULF OF SUEZ RIFT, EGYPT. Egyptian Journal of Geology, 63, 101–114.

Patton, T. L., Moustafa, A. R., Nelson, R. A., and Abdine, S. A. (1994). Tectonic evolution and structural setting of the Suez rift: chapter 1: Part I. Type basin: Gulf of Suez.

Pickett, G. R. (1972). Practical formation evaluation. GR Pickett.

Poupon, A., and Leveaux, J. (1971). Evaluation of water saturation in shaly formations. SPWLA Annual Logging Symposium, SPWLA–1971.

Radwan, A. E., Abdelghany, W. K., and Elkhawaga, M. A. (2021). Present-day in-situ stresses in Southern Gulf of Suez, Egypt: Insights for stress rotation in an extensional rift basin. Journal of Structural Geology, 147. https://doi.org/10.1016/j.jsg.2021.104334

Radwan, A. E., Abudeif, A. M., Attia, M. M., and Mohammed, M. A. (2019). Pore and fracture pressure modeling using direct and indirect methods in Badri Field, Gulf of Suez, Egypt. Journal of African Earth Sciences, 156. https://doi.org/10.1016/j.jafrearsci.2019.04.015

Ramadan, M. A. M., Abd El Hamed, A. G., Badran, F., and Nooh, A. Z. (2019). Relation between hydrocarbon saturation and pore pressure evaluation for the Amal Field area, Gulf of Suez, Egypt. Egyptian Journal of Petroleum, 28(1). https://doi.org/10.1016/j.ejpe.2018.04.005

Roberts, D. G. (2012). Regional Geology and Tectonics: Phanerozoic Rift Systems and Sedimentary Basins. In Regional Geology and Tectonics: Phanerozoic Rift Systems and Sedimentary Basins. https://doi.org/10.1016/C2010-0-67671-1

Shehata, A. A., Kassem, A. A., Brooks, H. L., Zuchuat, V., and Radwan, A. E. (2021). Facies analysis and sequence-stratigraphic control on reservoir architecture: Example from mixed carbonate/siliciclastic sediments of Raha Formation, Gulf of Suez, Egypt. Marine and Petroleum Geology, 131. https://doi.org/10.1016/j.marpetgeo.2021.105160

Stephens, D. B., Hsu, K. C., Prieksat, M. A., Ankeny, M. D., Blandford, N., Roth, T. L., Kelsey, J. A., and Whitworth, J. R. (1998). A comparison of estimated and calculated effective porosity. Hydrogeology Journal, 6(1). https://doi.org/10.1007/s100400050141.